



Supercapacitor performance of polymer-in-salt electrolyte/water-in-polymer salt electrolyte synthesized by complexing glutaraldehyde crosslinked corn starch with $\text{Mg}(\text{ClO}_4)_2$

Dipti Yadav¹ · Kamlesh Pandey² · Kanak Aggarwal¹ · Neelam Srivastava¹

Received: 30 April 2024 / Revised: 17 June 2024 / Accepted: 18 June 2024 / Published online: 3 July 2024
© The Author(s), under exclusive licence to Springer-Verlag GmbH Germany, part of Springer Nature 2024

Abstract

Energy devices with high energy/power density are the need of the day, and to achieve the same, electrolytes with faster ion transport and wider electrochemical stability window are required. Polymer-in-salt electrolytes (PISEs) are predicted to have the better required electrochemical properties in comparison to salt-in-polymer electrolytes (SIPES), but desired success is still to be achieved due to recrystallization problems. PISEs suffer from poor mechanical and/or electrochemical properties along with aging effects as well; hence, special efforts are required to reduce the crystallinity of PISEs. The present paper discusses a crosslinked corn starch complexed with $\text{Mg}(\text{ClO}_4)_2$ which not only has desired electrochemical properties but is also flexible. XRD study confirms the absence of crystalline nature, without any extra efforts to reduce it. Synthesized PISEs have high conductivity ($\sim 0.01 \text{ Scm}^{-1}$), wide ESW ($> 3 \text{ V}$), and low relaxation time (μs) along with being economical. Supercapacitors fabricated using this novel PISE with laboratory synthesized activated carbon (from leaves and corn starch) have shown good specific capacitance ($\sim 20 \text{ Fg}^{-1}$ and $\sim 45 \text{ Fg}^{-1}$, respectively). The power density is of the order of kW kg^{-1} , which is quite high in comparison to other reports. The shape of CV and LSV is strongly influenced by the salt concentration, i.e., by the ion-cluster size, and is also affected by the volume/size of the activated carbon pores.

Keywords Flexible PISE · Supercapacitor · High energy density · Wide ESW · Low relaxation time

Introduction

Energy devices with higher energy density and power density are required for different applications [1–7]. To enhance these two parameters, lots of efforts are being made by material scientists, to develop novel electrode and electrolyte materials. Great success has been achieved in the area of electrode material, but for better device performance, the scientific community still relies on liquid electrolytes, whenever new electrode performance has to be demonstrated [8–10]. Although some organic electrolyte and/or ionic liquid-based electrolytes [11–13] can operate at higher voltage, like all solid state electrolytes they suffer

from low conductivity. Also, the polymer electrolyte (which is commercially being used in many energy devices) suffers from slow ion transport and hence special efforts have to be made to achieve the desired properties. High performing energy devices with solid electrolytes are still a target to be achieved. In the 1990s [14], a new class of polymer electrolyte (polymer-in-salt electrolyte (PISE)) came into existence which is supposed to have faster ion conduction. Due to faster ion transport in PISEs, energy devices are expected to have a higher power density and hence these materials may be promising electrolytes for supercapacitor applications. The present paper aims to synthesize a novel ecofriendly and economical PISEs and to demonstrate its possible application in supercapacitor.

Polymer-in-salt electrolytes (PISEs) have received great attention because of their promising predicted characteristics of being free from disadvantages (like poor cation transference number and slower ion movement) of salt-in-polymer electrolyte (SIPES) [15–17]. Researchers have been working in the field since Angell et al. [18–20] reported that if the salt concentration is increased beyond the threshold value

✉ Neelam Srivastava
neel@bhu.ac.in

¹ Department of Physics (MMV Section), Banaras Hindu University, Varanasi, India

² National Centre of Experimental Mineralogy and Petrology, University of Allahabad, Allahabad, India

then, due to formation of continuous clusters throughout the matrix, cation transference number increases and ion transport becomes faster. These both are very favorable characteristics for the performance of energy devices. Still, these electrolytes have not achieved the desired success. The biggest constraint in achieving the commercial level PISEs is the recrystallization of salt [21], brittle lattice [22, 23] and aging effects [24]. Researchers are putting special efforts to reduce crystallinity by using different additives such as ZrO_2 [25], montmorillonite clays [26], graphene oxide [27], SiO_2 [28], halloysite nanoclay (HNC) [29], and LLZO [30] or by giving thermal treatment to enhance the electrochemical performance and to achieve morphology suitable for device fabrication. The present work is to achieve a stable soft-flexible high conducting PISE which is free from recrystallization problems without any special treatment.

Before selecting the host material, it is important to understand that the host requirement for SIPE and PISE is very different [31] and that is why the initial attempts to synthesize the PISE, using the SIPE's host, did not result in desired success. The reason for this is basically the role of the host in SIPEs and PISEs is different. In SIPE, the host polymer and salt interaction has to be strong enough so that host not only dissociates the salt but it controls the ion movement through its segmental motion [32–34], whereas in PISE host should be able to dissociate salt and hold the ions but the host-salt interaction should be weak enough to lead to polymer segmental motion decoupled ion transport [35, 36]. Moreover, the host should be ready to accommodate a large amount of salt without degrading the mechanical properties. The theoretical calculation indicates [37, 38] that molecules having loose bonding and/or hydrogen bonding may be a better host for PISEs, as this matrix facilitates cluster formation because of their loose and modifiable morphology.

Keeping all these in background and the fact that addition of salt breaks the starch into smaller [39] molecules which decreases the covalent bonding leading to increase in hydrogen bonding and providing new -OH and -H to interact with salt. This not only increases the salt acceptability but also, due to increasing hydrogen bonding which are weak, and can easily modify their length and strength as per the surroundings [40], facilitates the cluster formation. Starch being direct food for microorganisms has a tendency of fungal growth and hence instead of pristine starch our group preferred the glutaraldehyde (GA) crosslinked starch [41–43]. Crosslinked starch is not only free from fungus problems but it also results in soft and flexible morphology suitable for device fabrication.

$Mg(ClO_4)_2$ is used as dopant salt. The salt selection was biased by many factors: (i) limited availability of Li in future and hence we have to look for alternative cation, and in this race, sodium (Na) and magnesium (Mg) have

received greater attention [44–53]; (ii) Mg salt handling does not require too much precautions; (iii) Mg-S batteries [54–58] are being explored and hence its energy device fabrication processes are readily available to understand its suitability for device fabrications. Cost effectiveness is one of the most important factors for commercial application of any material. Simple and easy protocol without requiring sophisticated instruments will certainly make it more cost effective. Hence, in the present study, we have synthesized the material in ambient using a cost-effective simple solution cast technique protocol. PISEs have large amounts of salt; hence, their moisture content will certainly be high if they are not being handled in a closed atmosphere. Literature generally discusses Li-based PISEs which are operated in an inert atmosphere [59–66] and hence no reports could be found in the literature that if the material is prepared in ambient then how the water molecules will affect the conductivity and electrochemical stability window (ESW). The present PISE system is unique in the sense that although it has water content but, at the same time, ESW is wide. Hence, it may also be classified as water-in-polymer salt electrolyte (WiPSE) [40, 67–72].

Experimental section

Electrolyte preparation

For electrolyte preparation, procured chemicals were amylopectin rich-corn starch (CS) (Sigma Aldrich), $Mg(ClO_4)_2$ (Sigma Aldrich), methanol (Merck, India), and glutaraldehyde (GA) (Merck, India).

Simple solution cast technique was used for the synthesis of electrolytes of 65 wt% salt and 75 wt% salt, in ambient (34 °C room temperature and 45% RH). Total amount of corn starch and $Mg(ClO_4)_2$ in electrolyte was kept constant at 1 g. For the synthesis of electrolyte with 65 wt% salt, 10 ml methanol was taken in a beaker, and then, 0.35 g of corn starch and 0.7 ml of GA were added and magnetically stirred. In a separate beaker, 0.65 g of $Mg(ClO_4)_2$ salt was completely dissolved in 10 ml methanol by magnetic stirring. Then, $Mg(ClO_4)_2$ salt solution was added in the crosslinked corn starch solution. Obtained solution was continuously magnetically stirred for 5–6 h to get a homogeneous solution. This solution was poured in the petri dishes and was left for drying in the ambient. After 10 days, free-standing films were obtained as shown in Fig. 1. Similar synthesis procedure was followed for the electrolyte with 75 wt% salt. In this, 0.25 g of corn starch, 0.5 ml of GA and 0.75 g of $Mg(ClO_4)_2$ salt were added. Amount of crosslinker (GA) was optimized from the previous reports [49, 52]. For further discussions, electrolytes with 65wt% $Mg(ClO_4)_2$ and 75wt% $Mg(ClO_4)_2$ are named as S1 and S2, respectively.

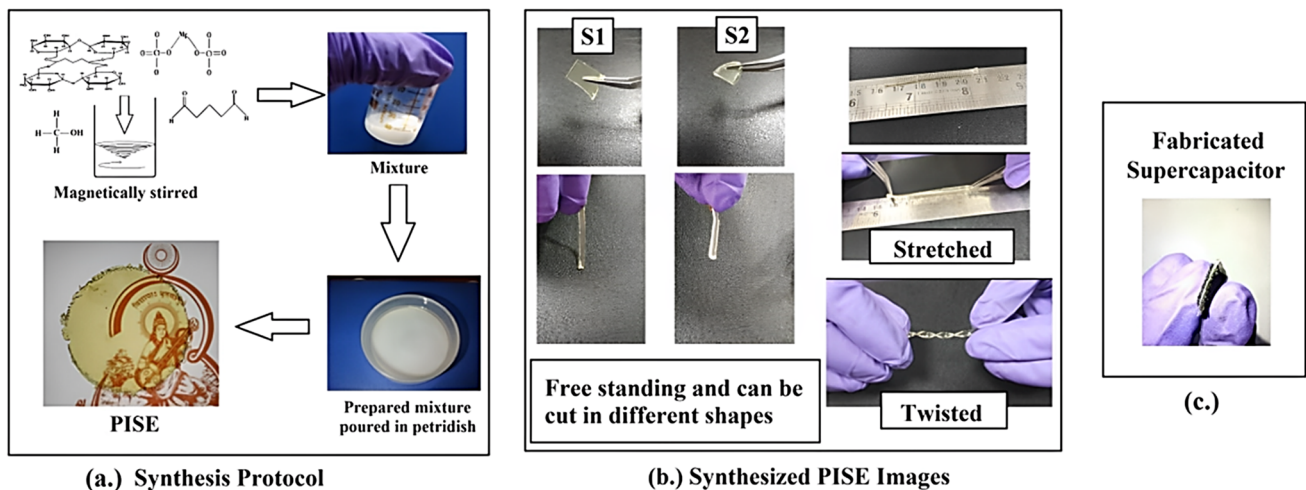


Fig. 1 **a** Schematic of PISE synthesis process. **b** Images of synthesized solid state PISE depicting flexibility, stretching, and freestanding nature of S1 and S2. **c** Image of fabricated supercapacitor

Effect of moisture on the electrochemical properties of the prepared electrolytes, S1 and S2, was critical as both corn starch and $\text{Mg}(\text{ClO}_4)_2$ are hydrophilic. Hence, a detailed attempt was made by treating S1 and S2 in different humidity atmospheres including exposure varying from 22 to 99% RH. This high humidity had forced the water molecules into the bulk of the electrolyte. ESR and moisture content were recorded at every step to understand the role/stability of water inside S1 and S2.

Electrode preparation

For the preparation of activated carbon, environment benign materials were selected, cornstarch and leaf. KOH was used for chemical activation [73, 74]. Corn starch (CS) was the same which was used in electrolyte synthesis and leaves were collected from the *Tectona grandis* tree in university campus. For making activated carbon, corn starch was directly used for pre-carbonization as received from the Sigma Aldrich and leaves were thoroughly washed multiple times with distilled water, dried, and crushed in fine powder before pre-carbonization. To prepare activated carbon from corn starch and leaves, a two-step activation process was followed. The first step was the pre-carbonization of the biomass at 600 °C in an inert atmosphere with the constant flow N_2 gas in a high temperature tube furnace. In the second step, pre-carbonized mass was mixed thoroughly with KOH in the ratio 1:2 and heated at 800 °C in an inert atmosphere with the constant flow of N_2 gas in a high temperature tube furnace. The obtained material was rinsed multiple times with diluted HCl and distilled water to remove the potassium remnants. Washed material was dried at 100 °C for 24 h to remove water. Material remaining after drying was the final activated carbon, used in the present study.

Electrodes were made by making slurry of activated carbon, PVA (binder), and carbon black Super P as a conductive agent which were mixed in a ratio of 8:1:1 in distilled water. Prepared slurry was coated on carbon cloth by using doctor's blade technique and was kept for drying at 100 °C for 12 h to remove water. Now onwards the activated carbon prepared from cornstarch and leaves was named as CAC and LAC, respectively.

Supercapacitor fabrication

Four supercapacitors were fabricated having a combination of two electrolytes S1 and S2 and two electrodes LAC and CAC. Fabricated supercapacitors were named as SC-LACS1, SC-LACS2, SC-CACS1, and SC-CACS2. Area of each electrode is 1 cm² with ~0.25 mg of active loaded mass (after the reduction of weight of binder and conductive agent) on each electrode and the commercial tissue paper (TP) was used as a separator. The configuration electrode/electrolyte/separator/electrolyte/electrode was used in all four cases (schematic of fabricated supercapacitor is shown in Fig. SM1 of Supplementary material (SM)).

Structural characterization

For the morphological characterization of the electrolyte, X-ray diffraction (XRD) patterns were recorded over the range of diffraction angle (2 theta) 5 to 80° using Bruker AXS (D2 Phaser) which employed Cu-K(alpha) radiation, with time/step of 2 s. Moisture content of S1 and S2 was measured using Mettler Toledo HS 153 Moisture Analyzer. For the surface morphology of the electrolyte, SEM micrographs were obtained from Jeol JXA 8100 (JAPAN) Electron Probe Micro Analyzer and Carl Zeiss EVO-18 Research Model (Scanning Electron

Microscope, Germany). Porosity, surface area, and pore volume of the activated carbon were found from the N_2 adsorption-desorption isotherm data (using Brunauer-Emmett-Teller (BET)) at 77.35 K from Autosorb iQ Station 1 instrument.

Electrochemical characterization

Electrochemical impedance spectroscopy analysis was carried out at applied voltage of 5 mV in the frequency range 1 mHz to 1 MHz. Linear sweep voltammetry (LSV), cyclic voltammetry (CV), and charging/discharging curves (GCD) of the supercapacitors were carried out by using CHI660E electrochemical workstation. Ionic conductivity of electrolyte was calculated by using the following equation:

$$\sigma = l/(R \times S)$$

where σ gives the conductivity in Scm^{-1} , R denotes the ESR in ohm of the electrolyte, l represents the thickness of the electrolyte, and S stands for surface area of the electrode/electrolyte contact in cm^2 . Specific capacitance C (Fg^{-1}) [75] was calculated by using the following formula:

$$C = (\int IdV)/(2mVs)$$

where C was the specific capacitance (Fg^{-1}), I was the current (A), dV was the differential voltage (V), m was the mass of loaded activated carbon, s was scan rate (Vs^{-1}), and V was the voltage range in which the CV has been recorded.

Specific energy density (E) and power density (P) [76] were calculated from the GCD curves by using the following formula:

$$E (\text{Wh kg}^{-1}) = 0.5CV^2/3.6$$

$$P (\text{W kg}^{-1}) = (E/t) 3600$$

where C was specific capacitance (Fg^{-1}), V was the potential change after IR drop, and t (s) was discharging time.

Result/discussion

Structural characterization of polymer-in-salt electrolyte (PISE)

Absence of phase separation patterns, in SEM micrographs shown in Fig. 2c–f, confirms homogeneous mixing of starch and salt and also confirms that there is no recrystallization of

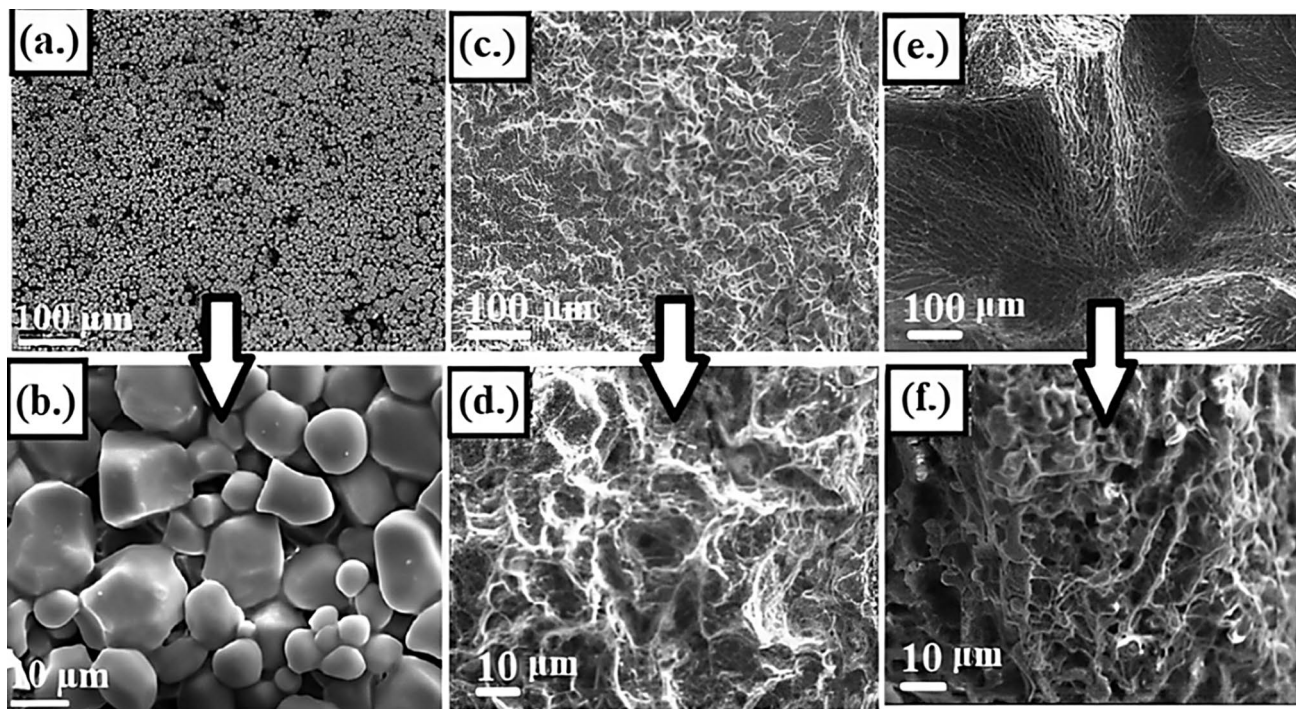


Fig. 2 SEM images of GA crosslinked cornstarch at resolutions **a** 100x (scale 100 μm) and **b** 500x (scale 10 μm), respectively. S1 electrolyte at resolution **c** 100x (scale 100 μm) and **d** 500x (scale

10 μm), respectively. S2 electrolyte at resolution **e** 100x (scale 100 μm) and **f** 500x (scale 10 μm), respectively

salt. Significant changes in morphology/texture are clearly visible on addition/increase in salt concentration. SEM micrographs are given at two different resolutions: (i) GA crosslinked starch, S1, and S2 at 100x magnification and (ii) GA crosslinked starch, S1, and S2 at 500x magnification to see the ion-cluster formation pattern. In Fig. 2a, b, granules are distinctly visible in crosslinked starch, which disappear after salt addition, confirming that salt breaks the starch granules. As discussed in report [39] because of this breaking of starch, which results in increasing the number of OH molecules to interact with cation and to enhance the hydrogen bonding resulting in increased amorphous nature and better acceptance of salt, crosslinked starch-based PISEs are free from crystallinity problems. Instead of these granule structures, a different type of morphology is seen in SEM micrographs of S1 and S2 at both resolutions (100x and 500x). The well-defined structures visible in Fig. 2d, f can be attributed to the formation of ion clusters. From the SEM micrographs at lower resolution (100x), Fig. 2c, e, where larger area is visible, it is clearly observed that S2 has a bigger ion-cluster (both in length and width) in comparison to S1. The impact of the bigger ion-cluster size has its impact in ESW estimation (details will be discussed in

the following section of “Performance of supercapacitors fabricated using CAC and LAC”).

At higher salt concentration, the salt recrystallization is an obvious phenomenon, in PISEs [77], which adversely affects the morphological and electrochemical properties of PISEs, and reducing the crystallinity at higher salt concentration is a great challenge for PISE synthesis. Researchers adopt different methodologies to bring the crystallinity to the lowest possible value [38, 78–81]. X-ray diffraction (XRD) pattern of the pure salt ($\text{Mg}(\text{ClO}_4)_2$), GA crosslinked corn starch (CS + GA), S1, and S2 is given in Fig. 3. Crystalline peaks and semi-crystalline peaks, respectively, visible in the XRD pattern of pure salt and CS + GA (GA crosslinked CS) have completely disappeared in S1 and S2. Amorphous nature is further enhanced with the increase in salt concentration from S1 to S2. The increasing amorphicity with increasing salt concentration without recrystallization of salt is a unique and favorable phenomenon as observed in the present system. Disappearance of salt characteristic peaks indicates the complete dissolution of salt in the crosslinked starch matrix. Hence, as mentioned above, the synthesized PISEs have an edge over the other reported PISEs, as no treatment is required to control recrystallization at higher salt concentration.

Fig. 3 XRD spectra of **a** pure magnesium perchlorate ($\text{Mg}(\text{ClO}_4)_2$) salt, **b** GA crosslinked corn starch, **c** S1 PISE, and **d** S2 PISE

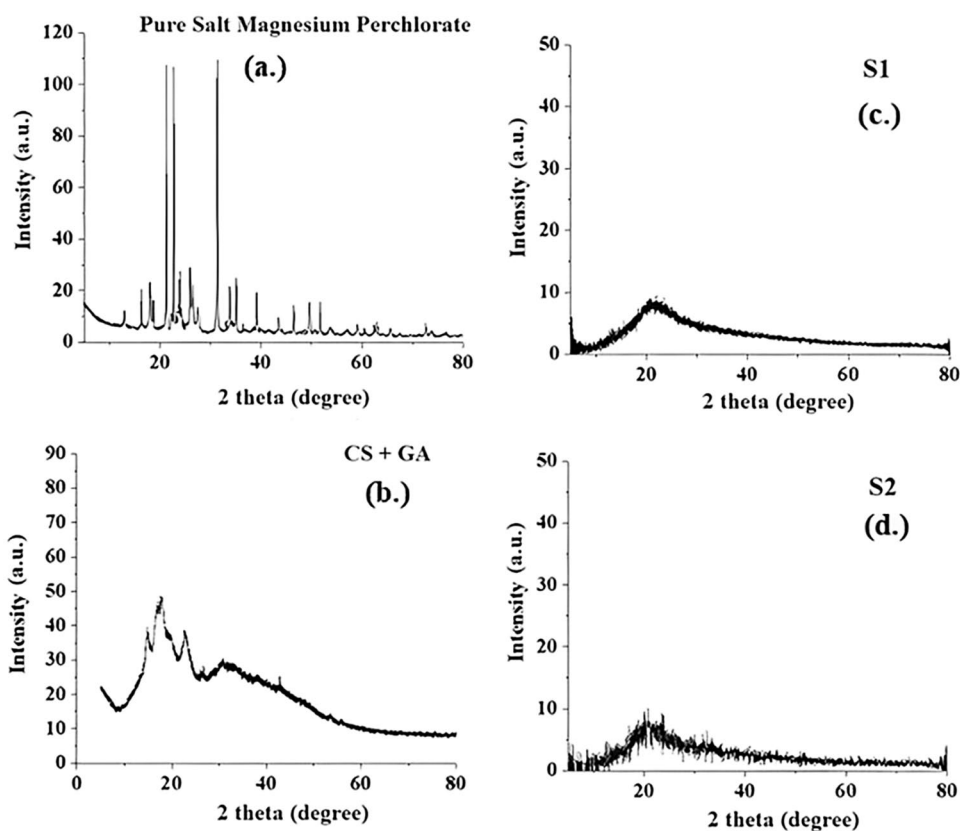


Table 1 ESR (Ω) and moisture content (%) study of S1 at different states of sample

S1	State of sample	ESR (ohm)	MC (%)
Step 1	Fresh sample (at 45% RH)	3.4	6.09
Step 2	Kept for 24 h at 22% RH	80,000	-2.91
Step 3	Kept for 24 h at 99% RH	3	51.92
Step 4	Kept for 24 h at 22% RH	7.6	3.88
Step 5	Again left in ambient for 24 h	3.9	21.82

ESR dependence on moisture

The PISEs have high salt concentration and hence are highly prone to water absorption, and in the present study, starch being hydrophilic host polymer adds up to it. Inspired by the water-in-polymer salt electrolyte (WiPSE) [40, 67–72] and method of using the diluents to enhance electrochemical and mechanical properties of PISEs [82–84], in the present study, instead of removing the water/moisture from synthesized PISEs, a reverse technique has been utilized, and by exposing the material to high humidity, the material's stability toward the ambient humidity has been increased. For understanding the effect of the ambient moisture, a detailed study of samples S1 and S2 has been carried out, where using impedance measurements in aluminum electrode/PISE/aluminum electrode cell configuration. Using a novel approach of exposing the synthesized material to high humidity by keeping it in a constant humidity chamber [85] for 24 h, the effect of high humidity exposure has been analyzed by measuring the impedance and moisture content, (i) fresh sample (RH~45%), (ii) keeping the sample in low humidity (RH~22%) for 24 h, (iii) exposing the sample to high humidity (RH~99%) for 24 h, and then again (iv) keeping the sample in low humidity chamber for 24 h. Tables 1 and 2 summarize the value of ESR and the detailed Nyquist plots (given as Fig. SM2), and moisture content (MC%) measurement curves are given as Supplementary material (given in Figs. SM3–SM12). Negligibly small negative value at step 2 is just because of the acceptance of water from the

Table 2 ESR (Ω) and moisture content (%) study of S2 at different states of sample

S2	State of sample	ESR (ohm)	MC (%)
Step 1	Fresh sample (at 45% RH)	1.5	18.26
Step 2	Kept for 24 h at 22% RH	453	-1.57
Step 3	Kept for 24 h at 99% RH	2	64.52
Step 4	Kept for 24 h at 22% RH	6.8	13.27
Step 5	Again left in ambient for 24 h	2.5	21.31

atmosphere during the heating process as the material is too dry. These results indicate that exposure to high humidity has an irreversible effect on conductivity and stabilizes the material with ambient humidity change, as observed by very small variation in resistance value. Slight increase in MC % after step (iv) indicates that high humidity exposure resulted in some well bonded molecules which do not come out of the matrix by keeping the material at low RH, indicating that present PISE is quite stable.

The absorbed water seems to play the role of diluent [82] and stabilizes the conductivity value. The ambient measurements have been repeated multiple times in the duration of 6 months and the resistance is within 3–5 Ω (for S1) and 1–3 Ω (for S2). The presence of water helps in maintaining its flexible nature which adds up to ease of cutting these PISEs into different shapes and sizes for device fabrication (Fig. 1). This absorbed water is electrochemically stable and does not break at low potential as indicated by LSV studies in the following section of “Performance of supercapacitors fabricated using CAC and LAC”.

Structural analysis of laboratory synthesized activated carbons

In the present study, activated carbons have been synthesized using cornstarch and leaf as initial material. The structural analysis of CAC and LAC has been carried out using SEM and BET techniques to understand their morphology and pore size/surface area. SEM images of the CAC and LAC are given in Fig. 4a, b at the same scale of 200 nm. CAC is observed to have greater surface area as compared to LAC, which has its impact on supercapacitor behavior.

Surface area and the porosity analysis of the CAC and LAC have been done by N_2 -sorption isotherms at 77 K (detailed parameters are mentioned in Tables SM1–SM4 of Supplementary material) as shown in Fig. 4c, d. Surface area, pore volume, and pore radius values of the LAC and CAC are shown in Table 3. According to IUPAC classification, CAC and LAC show type IV isotherms. Type IV isotherms correspond to microporous solids with relatively small external surface area and attributes to mesoporous structures where capillary condensation of liquid nitrogen takes place [86].

Volume of nitrogen adsorbed in CAC is relatively higher than in LAC which indicates high porosity of CAC. The initial slight rise in both the isotherms of CAC and LAC indicates the little uptake of nitrogen at low relative pressure for the formation of monolayer in different sized pores. Further, the slope of the isotherm gradually increases with the pressure leading to the formation of a hysteresis loop during N_2 desorption indicating the mesoporous interiors in isotherms of CAC and LAC.

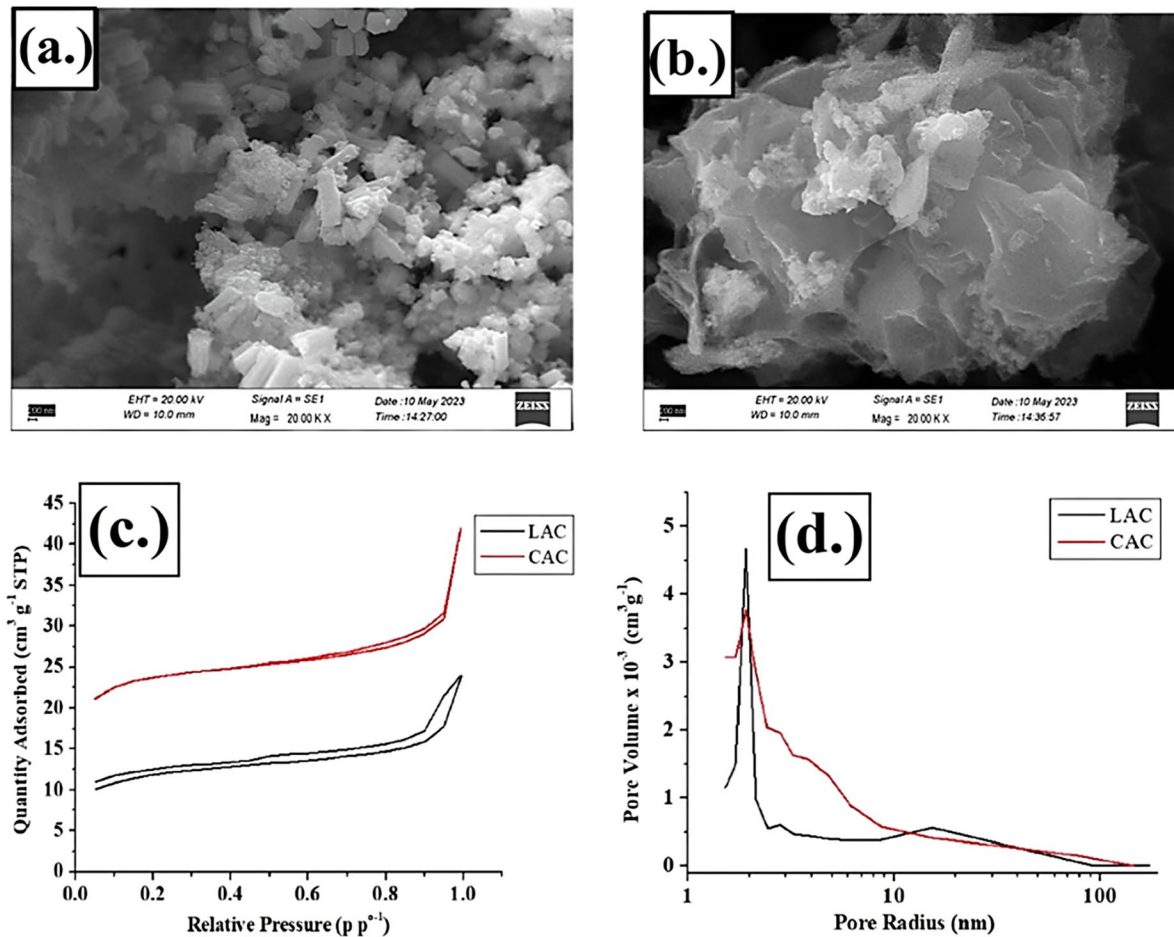


Fig. 4 **a** SEM image of activated carbon synthesized from cornstarch (CAC). **b** SEM image of activated carbon synthesized from leaf (*Tectona grandis*) (LAC). **c** N_2 -adsorption-desorption isotherm of LAC and CAC. **d** Pore size distribution curve of LAC and CAC

Different types of hysteresis loops are observed in type IV isotherms which attributes to specific pore structures. CAC exhibits type H3 loop indicating aggregates of plate-like particles that give rise to slit-shaped pores, cracks, and wedge structure. LAC exhibits type H4 loop, which is associated with narrow slit-like pores but the adsorption-desorption isotherm does not overlap at low pressure attributing to micropores. H4 hysteresis also occurs over solids containing micropores, mesopores, and narrow cracked pores [87]. This low pressure hysteresis may be

Table 3 Characteristics of pore structures of synthesized activated carbon, LAC and CAC

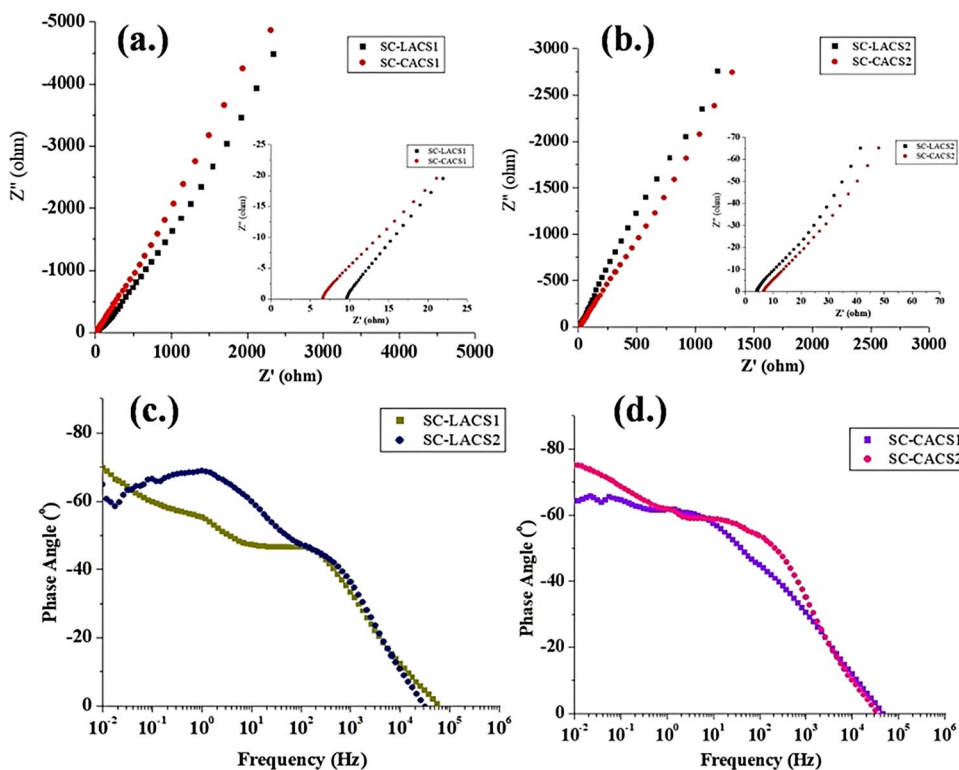
Sample type	Surface area (m^2g^{-1})	Pore volume (cm^3g^{-1})	Pore radius (nm)
LAC (<i>adsorption</i>)	30.881	0.134	1.5284
LAC (<i>desorption</i>)	40.077	0.133	1.9105
CAC (<i>adsorption</i>)	57.994	0.324	1.7065
CAC (<i>desorption</i>)	76.692	0.335	1.9098

observed extending to the lowest attainable pressure which is due to the residual adsorbed N_2 in the pores attributing to the swelling of a non-rigid porous structure or irreversible uptake of molecules in pores. This residual N_2 can be removed by out-gassing adsorbent at higher temperatures [86].

Performance of supercapacitors fabricated using CAC and LAC

Carbon cloth is used to prepare the electrodes for supercapacitor fabrication; hence, four different supercapacitors are fabricated (i) LAC/S1/TP/S1/LAC (SC-LACS1), (ii) LAC/S2/TP/S2/LAC (SC-LACS2), (iii) CAC/S1/TP/S1/CAC (SC-CACS1), and (iv) CAC/S2/TP/S2/CAC (SC-CACS2), (i) and (ii) carbon cloth loaded with LAC and (iii) and (iv) carbon cloth loaded with CAC. In all these supercapacitors (SC), tissue paper (TP) is used as a separator. To estimate the ESR value of fabricated supercapacitors, the Nyquist plots have been used as shown in Fig. 5a, b. ESR values

Fig. 5 Nyquist plot of fabricated supercapacitors. **a** SC-LACS1 and SC-CACS1. **b** SC-LACS2 and SC-CACS2. Bode plots of fabricated supercapacitors. **c** SC-LACS1 and SC-LACS2. **d** SC-CACS1 and SC-CACS2



are tabulated in Table 4. Figure 5c, d shows the Bode phase plots for the system. The phase angle approaches to nearly 80° which is indicative of the capacitance dominating nature of the system.

The ESR value remains below $10\ \Omega$ for S1 electrolyte and for S2 it is below $6\ \Omega$, with a nominal difference with the electrode variation. The absence of the semicircle is indicative of the fast ion transport [88, 89] and dominance of capacitive behavior. Slope of the Nyquist plots is observed to be higher with S2 electrolyte as compared to S1 electrolyte, indicating the relatively high capacitance achieved with S2.

ESW [90–93] of all the six fabricated supercapacitors are estimated using LSV measurements and are shown in Fig. 6. The electrochemical stability window (ESW) of

supercapacitor fabricated from Pristine Carbon Cloth (PCC) reduces from 4 to 3 V for SC-PCCS1 (PCC/S1/TP/S1/PCC (SC-PCCS1)) and SC-PCCS2 (PCC/S2/TP/S2/PCC (SC-PCCS1)). In the presence of coated activated carbon, quite a large decrease in ESW has been observed. ESW for SC-LACS1 is 3.4 V and for SC-LACS2 it has reduced to ~ 1 V, whereas the ESW for SC-CACS1 and SC-CACS2 is 2.5 V and ~ 1 V, respectively. The probable causes of lower value of ESW for S2 based SCs may be caused by either (i) the presence of water in PISEs and/or (ii) it may be an ion (or cluster) size effect. The first option is ruled out by the ESW studies of SC-PCCS1 and SC-PCCS2 as the ESW is quite wide in these cases, indicating that PISEs S1 and S2 are stable and no water electrolysis is observed. Literature [94] indicates that ESW width strongly depends upon the size of ion/ion clusters and pore size. Considering a particular supercapacitor system, a clear decrease in ESW from SC-PCCS1 to SC-PCCS2 is an obvious result because, with increasing salt concentration, increasing size of ion cluster is expected as confirmed by SEM micrographs. This phenomenon is invariably observed with all the three electrode systems selected in the present study. Shilina et al. [95] have correlated the phenomenon of decreased ESW with increased ion size in terms of initiation of side reaction. Stripping off of ion cluster [94] may also be a reason for decreased ESW in case of S2. Longer ion clusters are more prone to break at the electrode/electrolyte interface during polarization as compared to shorter ion clusters.

Table 4 Electrochemical parameters of fabricated supercapacitors from CV, SC-LACS1, SC-LACS2, SC-CACS1, and SC-CACS2

Fabricated supercapacitor	ESR (ohm)	Relaxation time (ms)	Calculation from CV data at scan rate $1\ \text{mVs}^{-1}$	
			Specific capacitance (Fg^{-1})	Energy density (Wh kg^{-1})
SC-LACS1	10.12	10	13	1.8
SC-LACS2	4.09	5.7	20	2.7
SC-CACS1	7.25	4.6	41	5.7
SC-CACS2	5.73	2.1	45	6.25

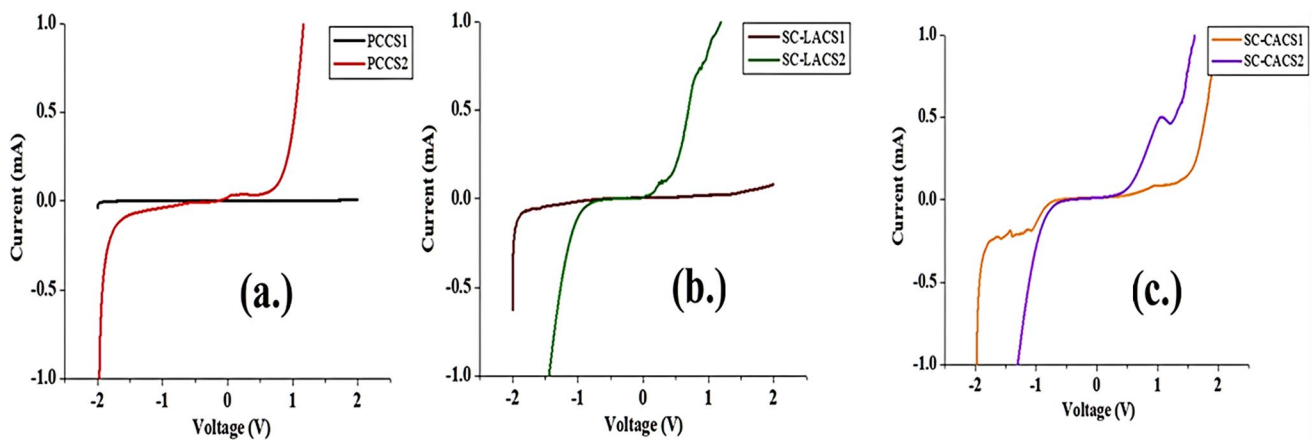


Fig. 6 Electrochemical stability window (ESW) of **a** SC-PCCS1 and SC-PCCS2, **b** SC-LACS1 and SC-LACS2, and **c** SC-CACS1 and SC-CACS2

Electrode/electrolyte interfaces are crucial to understand the charge storage mechanisms in the supercapacitor systems. Reorganization of structure of ions and their adsorption at the electrode decide the capacitive behavior of the system. In the water-in-polymer salt electrolytes (WiPSEs), which are studied here, understanding of ionic arrangements in the electrolyte is yet to be established [40, 67–72]. Applicability of WiPSEs for supercapacitor applications is not

much explored and is quite new. Value of relaxation time of the fabricated SCs is shown in Table 4, and analysis is mentioned in Supplementary material under the section Frequency-dependent capacitive behavior with Fig. SM14.

Herein, an attempt is made to understand the governing mechanisms. Cyclic voltammograms for SC-LACS1, SC-LACS2, SC-CACS1, and SC-CACS2 are shown in Fig. 7. Specific capacitances are estimated by using the

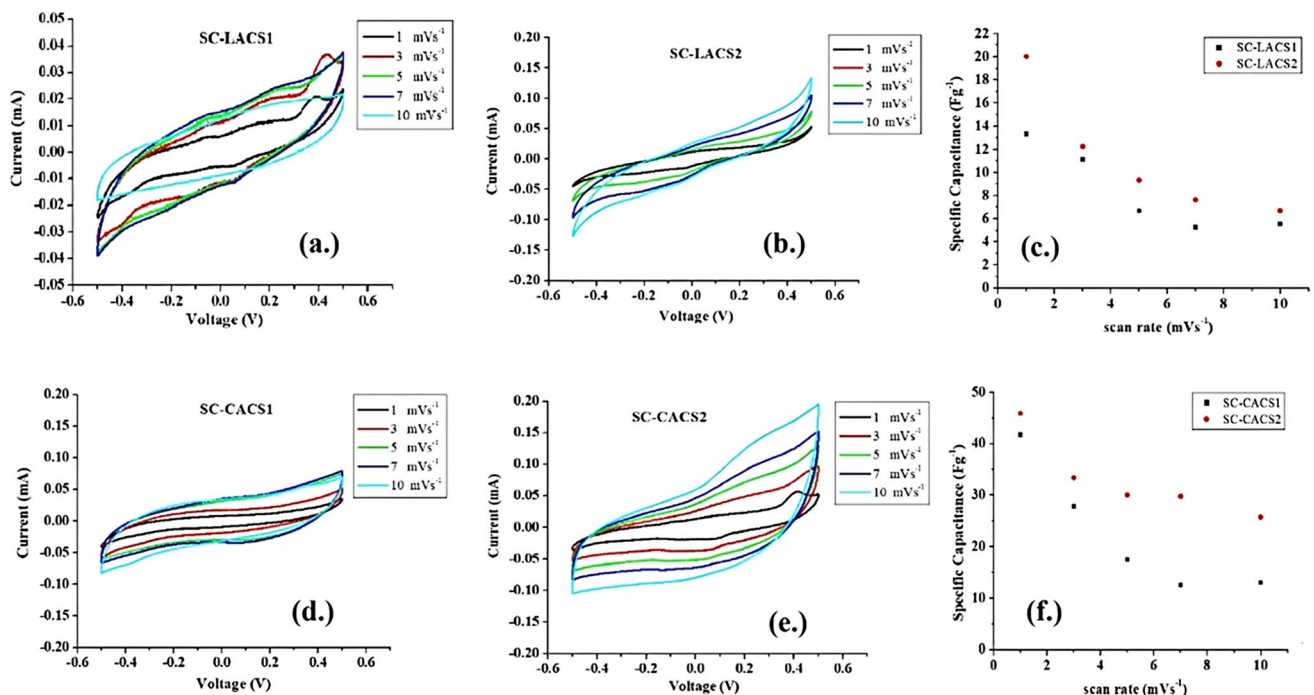


Fig. 7 Cyclic voltammograms of fabricated supercapacitor from scan rate of 1 to 10 mVs^{-1} **a** SC-LACS1 and **b** SC-LACS2. **c** Variation of specific capacitance with scan rate of 1 to 10 mVs^{-1} of SC-LACS1

and SC-LACS2. Cyclic voltammograms of fabricated supercapacitor from scan rate of 1 to 10 mVs^{-1} **d** SC-CACS1 and **e** SC-CACS2. **f** Variation of specific capacitance with scan rate of 1 to 10 mVs^{-1}

formula mentioned in “Experimental section” at the scan rate of 1 mVs^{-1} in the potential range of -0.5 to $+0.5 \text{ V}$ [49, 52, 96–98].

As mentioned in the ESW section, reorganization of the ion clusters at the electrode/electrolyte interface might be the dominating process in the capacitive behavior. SC fabricated using S2 has higher specific capacitance in comparison to SC fabricated using S1. This might be correlated with the size of ion clusters and their adsorption at the pores of electrodes. In S1, ion cluster size of SC-CACS1 and SC-CACS2 is small, as can be observed from the SEM micrographs, as compared to S2. A smaller effective ion cluster being adsorbed at the larger pore leads to some vacant space resulting in lower capacitance [99, 100]. With the increase in the effective size of the ion clusters, vacant space of the carbon pores get filled and effective distance between pore wall

and ion cluster decreases, leading to the increased specific capacitance (as shown in Fig. SM13 of Supplementary material) [101, 102].

Cyclic ability of the electrode/electrolyte interface of the supercapacitor system is analyzed by performing charging/discharging at constant current density of 4 Ag^{-1} from -0.5 to $+0.5 \text{ V}$ for 3000 cycles. Coulombic efficiency of the fabricated supercapacitors is shown in Fig. 8. The coulombic efficiency ($\eta\%$) is evaluated from the expression [103–106] $\eta = t_d/t_c \times 100\%$, where t_c and t_d are the time of charging and discharging of the cell, respectively, at a constant current. Coulombic efficiency of fabricated supercapacitors is observed to be $> 95\%$ [107]. Charging/discharging of fabricated supercapacitors at different current densities (from 4 to 36 Ag^{-1}) is shown in Fig. 8a–f. The estimated energy density and power density from

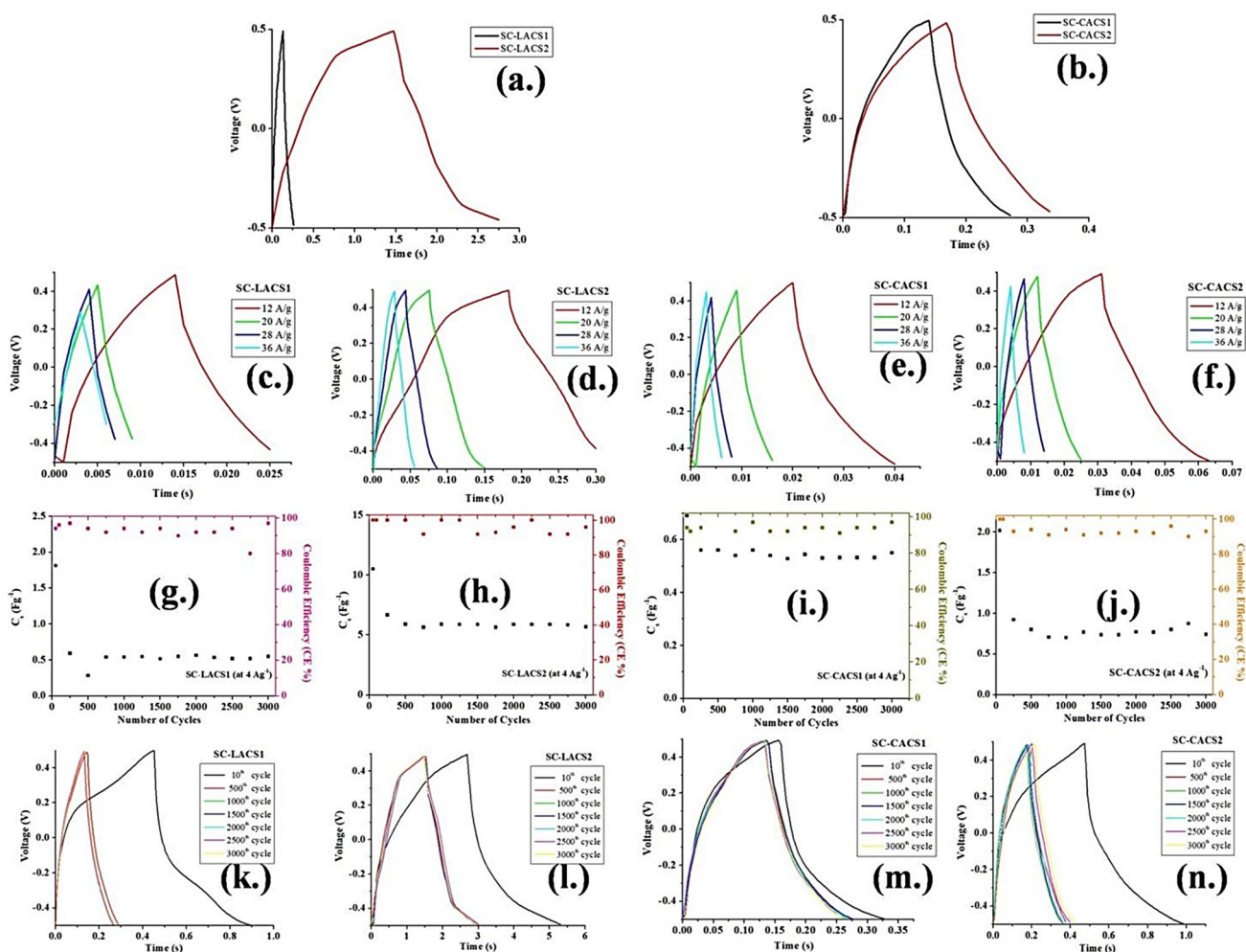


Fig. 8 Charge-discharge cycles at 4 Ag^{-1} of **a** SC-LACS1 and SC-LACS2 and **b** SC-CACS1 and SC-CACS2. Charge-discharge cycles from 12 to 36 Ag^{-1} of **c** SC-LACS1, **d** SC-LACS2, **e** SC-CACS1, and **f** SC-CACS2. Cyclic behavior of coulombic efficiency (CE) and

specific capacitance at 4 Ag^{-1} of **g** SC-LACS1, **h** SC-LACS2, **i** SC-CACS1, and **j** SC-CACS2. Cyclic stability of **k** SC-LACS1, **l** SC-LACS2, **m** SC-CACS1, and **n** SC-CACS2

Table 5 Electrochemical parameters of fabricated supercapacitors from charging/discharging data, SC-LACS1, SC-LACS2, SC-CACS1, and SC-CACS2

Fabricated supercapacitor	Calculation from GCD data at current density 4 Ag ⁻¹		
	Specific capacitance (Fg ⁻¹)	Energy density (Wh kg ⁻¹)	Power density (kW kg ⁻¹)
SC-LACS1	0.48	0.069	2.1
SC-LACS2	5.2	0.72	1.9
SC-CACS1	0.4	0.06	2.2
SC-CACS2	0.6	0.08	1.9

these curves are mentioned in Table 5. Figure 8g–j indicates the cyclic behavior of coulombic efficiency and capacitance value. Stability of cyclic behavior of charging/discharging curves is demonstrated in Fig. 8k–n by showing curves at selected cycles.

As expected, since the faster ion transfer is observed in PISEs, hence the power density value is quite high. Both the estimated values are similar to those reported in literature for similar systems as summarized in Table SM5 of Supplementary material [108–113].

Conclusion

Using an economical synthesis protocol, flexible PISEs have been synthesized having GA crosslinked corn starch doped Mg(ClO₄)₂ salt. The special feature of synthesis protocol and selected chemicals is that it is free from the need of having the eutectic salt/mixture and/or any other additive to achieve the desired mechanical and electrochemical properties. PISEs have high salt concentration and are prone to water absorption. Its stability toward ambient humidity changes has been improved by using a unique technique of exposing the sample to high humidity. PISEs have a wide electrochemical stability window (> 3 V) even with high moisture content. Supercapacitors fabricated using laboratory synthesized activated carbon (synthesized from leaves and corn starch) have shown good specific capacitance (~20 Fg⁻¹ and ~45 Fg⁻¹, respectively) and energy density for SC-LACS1, SC-LACS2, SC-CACS1, and SC-CACS2, 1.8 Wh kg⁻¹, 2.7 Wh kg⁻¹, 5.7 Wh kg⁻¹, and 6.25 Wh kg⁻¹. Coulombic efficiency is more than 95%, and shorter charging/discharging time resulted in high power density for SC-LACS1, SC-LACS2, SC-CACS1, and SC-CACS2, 2.1 kW kg⁻¹, 1.9 kW kg⁻¹, 2.2 kW kg⁻¹, and 1.9 kW kg⁻¹, respectively, which is possible because of the faster ion transport in PISEs. All these results indicate that the GA crosslinked starch-based PISE is a potential candidate for

future energy devices, which being cost-effective, easy to handle, and easy to synthesize PISE may reach to commercial level, if explored in greater detail.

Supplementary Information The online version contains supplementary material available at <https://doi.org/10.1007/s10008-024-05982-8>.

Acknowledgements The authors acknowledge the Central Instrumentation Lab facility (CIL, MMV BHU) for XRD measurements, Dr. Vikas Kumar Das for permitting access to the N₂-sorption isotherms (BET facility) at Departmental Instrumentation Facility of Department of Chemistry (BHU), Prof. NV Chalapathi Rao for permitting access to SEM facility at Centre of Advanced Study in Geology (BHU), and Dr. Kamlesh Pandey (University of Allahabad, Prayagraj) for providing the SEM facility.

Funding Author NS is thankful to BHU for providing research incentive grant for faculty (IoE scheme) Dev scheme No 6031-sanction number R/Dev/D/IoE/Incentive/2021-22/32161 and also an infrastructure grant sanction number R/Dev/D/Object head 35/2018-19/73496. Authors DY and KA are thankful to Banaras Hindu University for UGC research fellowship. BHU administration is thankfully acknowledged for providing the fund for CHI660E instrument.

References

1. Pal B, Yang S, Ramesh S, Thangadurai V, Jose R (2019) Electrolyte selection for supercapacitive devices: A critical review. *Nanoscale Advances* 1(10):3807–3835
2. Pal B, Yasin A, Kaur R, Tebyetekerwa M, Zabihi F, Yang S, Yang CC, Sofer Z, Jose R (2021) Understanding electrochemical capacitors with in-situ techniques. *Renew Sustain Energy Rev* 149:111418
3. Saini S, Chand P, Joshi A (2021) Biomass derived carbon for supercapacitor applications. *J Energy Storage* 39:102646
4. Ali Z, Iqbal MZ, Hegazy HH (2023) Recent advancements in redox-active transition metal sulfides as battery-grade electrode materials for hybrid supercapacitors. *J Energy Storage* 73:108857
5. Ren W, Ding C, Fu X, Huang Y (2021) Advanced gel polymer electrolytes for safe and durable lithium metal batteries: Challenges, strategies, and perspectives. *Energy Storage Mater* 34:515–535
6. Srivastava N, Kumar M (2016) Ion dynamics and relaxation behavior of NaPF₆-doped polymer electrolyte systems. *J Solid State Electrochem* 20:1421–1428
7. Zhao Z, Huang Y, Ren W, Zhao L, Li X, Wang M, Lin Y (2021) Natural biomass hydrogel based on cotton fibers/PVA for acid supercapacitors. *ACS Appl Energy Mater* 4(9):9144–9153
8. Salama RS, Gouda MS, Aboud MFA, Alshorifi FT, El-Hallag AA, Badawi AK (2024) Synthesis and characterization of magnesium ferrite-activated carbon composites derived from orange peels for enhanced supercapacitor performance. *Sci Rep* 14:8223
9. Liao H, Zhong L, Zeng H, Xiao Y, Cheng B, Lei S (2024) Dual-function highly oxidative potassium salts empowering high-performance transition metal oxide/activated carbon for hybrid aqueous supercapacitors. *Carbon* 224:119080
10. Abioye AM, Ani FN (2015) Recent development in the production of activated carbon electrodes from agricultural waste biomass for supercapacitors: A review. *Renew Sustain Energy Rev* 52:1282–1293

11. Pang L, Wang H (2022) Inorganic aqueous anionic redox liquid electrolyte for supercapacitors. *Adv Mater Technol* 7(4):2100501
12. Lan S, Yu C, Yu J, Zhang X, Liu Y, Xie Y, Wang J, Qiu J (2024) Recent advances in low-temperature liquid electrolyte for supercapacitors. *Small* 2309286. <https://doi.org/10.1002/sml.202309286>
13. Béguin F, Presser V, Balducci A, Frackowiak E (2014) Carbons and electrolytes for advanced supercapacitors. *Adv Mater* 26(14):2219–2251
14. Angell CA, Liu C, Sanchez E (1992) A new type of cation-conducting rubbery solid electrolyte: The ionic rubber. *MRS Online Proceedings Library (OPL)* 293:75
15. Yue L, Ma J, Zhang J, Zhao J, Dong S, Liu Z, Cui G, Chen L (2016) All solid-state polymer electrolytes for high-performance lithium ion batteries. *Energy Storage Mater* 5:139–164
16. Wischniewski A, Monkenbusch M, Willner L, Richter D, Kali G (2003) Direct observation of the transition from free to constrained single-segment motion in entangled polymer melts. *Phys Rev Lett* 90(5):058302
17. Xue Z, He D, Xie X (2015) Poly (ethylene oxide)-based electrolytes for lithium-ion batteries. *J Mater Chem A* 3(38):19218–19253
18. Angell CA, Liu C, Sanchez E (1993) Rubbery solid electrolytes with dominant cationic transport and high ambient conductivity. *Nature* 362(6416):137–139
19. Fan J, Angell CA (1995) The preparation, conductivity, viscosity and mechanical properties of polymer electrolytes and new hybrid ionic rubber electrolytes. *Electrochim Acta* 40(13–14):2397–2400
20. Xu K, Xu W, Zhang SS (2022) Austen Angell’s legacy in electrolyte research. *J Non-Crystalline Solids X* 14:100088
21. Zalewska A, Pruszczyk I, Sułek E, Wiecezorek W (2003) New poly (acrylamide) based (polymer in salt) electrolytes: Preparation and spectroscopic characterization. *Solid State Ionics* 157(1–4):233–239
22. Florjańczyk Z, Zygadło-Monikowska E, Wiecezorek W, Ryszawy A, Tomaszewska A, Fredman K, Golodnitsky D, Peled E, Scrosati B (2004) Polymer-in-salt electrolytes based on acrylonitrile/butyl acrylate copolymers and lithium salts. *J Phys Chem B* 108(39):14907–14914
23. Zhang X, Liu T, Zhang S, Huang X, Xu B, Lin Y, Xu B, Li L, Nan CW, Shen Y (2017) Synergistic coupling between Li₆. 75La₃Zr₁. 75Ta₀. 25O₁₂ and poly (vinylidene fluoride) induces high ionic conductivity, mechanical strength, and thermal stability of solid composite electrolytes. *J Am Chem Soc* 139(39):13779–13785
24. Łasińska AK, Marzantowicz M, Dygas JR, Krok F, Florjańczyk Z, Tomaszewska A, Zygadło-Monikowska E, Żukowska Z, Lafont U (2015) Study of ageing effects in polymer-in-salt electrolytes based on poly (acrylonitrile-co-butyl acrylate) and lithium salts. *Electrochim Acta* 169:61–72
25. Sheng O, Jin C, Luo J, Yuan H, Fang C, Huang H, Gan Y, Zhang J, Xia Y, Liang C, Zhang W (2017) Ionic conductivity promotion of polymer electrolyte with ionic liquid grafted oxides for all-solid-state lithium–sulfur batteries. *J Mater Chem A* 5(25):12934–12942
26. Zhang Y, Zhao Y, Gosselink D, Chen P (2015) Synthesis of poly (ethylene-oxide)/nanoclay solid polymer electrolyte for all solid-state lithium/sulfur battery. *Ionics* 21:381–385
27. Jia W, Li Z, Wu Z, Wang L, Wu B, Wang Y, Cao Y, Li J (2018) Graphene oxide as a filler to improve the performance of PAN-LiClO₄ flexible solid polymer electrolyte. *Solid State Ionics* 315:7–13
28. Choudhury S, Choudhury S (2019) A highly reversible room-temperature lithium metal battery based on cross-linked hairy nanoparticles. Rational design of nanostructured polymer electrolytes and solid–liquid Interphases for lithium batteries 35–57. https://doi.org/10.1007/978-3-030-28943-0_3
29. Lin Y, Wang X, Liu J, Miller JD (2017) Natural halloysite nanoclay electrolyte for advanced all-solid-state lithium-sulfur batteries. *Nano Energy* 31:478–485
30. Chen L, Li Y, Li SP, Fan LZ, Nan CW, Goodenough JB (2018) PEO/garnet composite electrolytes for solid-state lithium batteries: From “ceramic-in-polymer” to “polymer-in-ceramic”. *Nano Energy* 46:176–184
31. Wang Z, Gao W, Chen L, Mo Y, Huang X (2002) Study on roles of polyacrylonitrile in “salt-in-polymer” and “polymer-in-salt” electrolytes. *Solid State Ionics* 154:51–56
32. Jankowsky S, Hiller MM, Wiemhöfer HD (2014) Preparation and electrochemical performance of polyphosphazene based salt-in-polymer electrolyte membranes for lithium ion batteries. *J Power Sources* 253:256–262
33. Grünebaum M, Hiller MM, Jankowsky S, Jeschke S, Pohl B, Schürmann T, Vettikuzha P, Gentschev AC, Stolina R, Müller R, Wiemhöfer HD (2014) Synthesis and electrochemistry of polymer based electrolytes for lithium batteries. *Prog Solid State Chem* 42(4):85–105
34. Karatas Y, Banhatti RD, Kaskhedikar N, Burjanadze M, Funke K, Wiemhöfer HD (2009) Synthesis and modeling of polysiloxane-based salt-in-polymer electrolytes with various additives. *J Phys Chem B* 113(47):15473–15484
35. Mindemark J, Lacey MJ, Bowden T, Brandell D (2018) Beyond PEO—alternative host materials for Li⁺-conducting solid polymer electrolytes. *Prog Polym Sci* 81:114–143
36. Liu W, Yi C, Li L, Liu S, Gui Q, Ba D, Li Y, Peng D, Liu J (2021) Designing polymer-in-salt electrolyte and fully infiltrated 3D electrode for integrated solid-state lithium batteries. *Angew Chem* 133(23):13041–13050
37. Wu H, Gao P, Jia H, Zou L, Zhang L, Cao X, Engelhard MH, Bowden ME, Ding MS, Hu J, Hu D (2021) A polymer-in-salt electrolyte with enhanced oxidative stability for lithium metal polymer batteries. *ACS Appl Mater Interfaces* 13(27):31583–31593
38. Chen F, Wang X, Armand M, Forsyth M (2022) Cationic polymer-in-salt electrolytes for fast metal ion conduction and solid-state battery applications. *Nat Mater* 21(10):1175–1182
39. Moreau L, Bindzus W, Hill S (2011) Influence of salts on starch degradation: Part II—salt classification and caramelisation. *Starch-Stärke* 63(11):676–682
40. Samanta P, Ghosh S, Kolya H, Kang CW, Murmu NC, Kuila T (2021) Molecular crowded “water-in-salt” polymer gel electrolyte for an ultra-stable Zn-ion battery. *ACS Appl Mater Interfaces* 14(1):1138–1148
41. Li B, Shan CL, Zhou Q, Fang Y, Wang YL, Xu F, Han LR, Ibrahim M, Guo LB, Xie GL, Sun GC (2013) Synthesis, characterization, and antibacterial activity of cross-linked chitosan-glutaraldehyde. *Mar Drugs* 11(5):1534–1552
42. Yu Q, Song Y, Shi X, Xu C, Bin Y (2011) Preparation and properties of chitosan derivative/poly (vinyl alcohol) blend film crosslinked with glutaraldehyde. *Carbohydr Polym* 84(1):465–470
43. Bursali EA, Coskun S, Kizil M, Yurdakoc M (2011) Synthesis, characterization and in vitro antimicrobial activities of boron/starch/polyvinyl alcohol hydrogels. *Carbohydr Polym* 83(3):1377–1383
44. Bitner-Michalska A, Nolis GM, Żukowska G, Zalewska A, Poteła M, Trzeciak T, Dranka M, Kalita M, Jankowski P, Niedzicki L, Zachara J (2017) Fluorine-free electrolytes for all-solid sodium-ion batteries based on percyano-substituted organic salts. *Sci Rep* 7(1):40036
45. Osman Z, Md Isa KB, Ahmad A, Othman L (2010) A comparative study of lithium and sodium salts in PAN-based ion conducting polymer electrolytes. *Ionics* 16:431–435

46. Yang J, Zhang H, Zhou Q, Qu H, Dong T, Zhang M, Tang B, Zhang J, Cui G (2019) Safety-enhanced polymer electrolytes for sodium batteries: Recent progress and perspectives. *ACS Appl Mater Interfaces* 11(19):17109–17127
47. Boschin A, Johansson P (2015) Characterization of NaX (X: TFSI, FSI)–PEO based solid polymer electrolytes for sodium batteries. *Electrochim Acta* 175:124–133
48. Gebert F, Knott J, Gorkin R III, Chou SL, Dou SX (2021) Polymer electrolytes for sodium-ion batteries. *Energy Storage Materials* 36:10–30
49. Yadav M, Kumar M, Srivastava N (2018) Supercapacitive performance analysis of low cost and environment friendly potato starch based electrolyte system with anodized aluminium and teflon coated carbon cloth as electrode. *Electrochim Acta* 283:1551–1559
50. Sundermann DA, Park B, Hirschberg V, Schaefer JL, Théato P (2023) Magnesium polymer electrolytes based on the polycarbonate poly (2-butyl-2-ethyltrimethylene-carbonate). *ACS Omega* 8(26):23510–23520
51. Park B, Schaefer JL (2020) Polymer electrolytes for magnesium batteries: Forging away from analogs of lithium polymer electrolytes and towards the rechargeable magnesium metal polymer battery. *J Electrochem Soc* 167(7):070545
52. Yadav M, Kumar M, Srivastava N (2023) High-conducting, economical, and flexible polymer-in-salt electrolytes (PISEs) suitable for energy devices: A reality due to glutaraldehyde crosslinked starch as host. *J Solid State Electrochem* 27(5):1213–1226
53. Viviani M, Meereboer NL, Saraswati NLP, Loos K, Portale G (2020) Lithium and magnesium polymeric electrolytes prepared using poly (glycidyl ether)-based polymers with short grafted chains. *Polym Chem* 11(12):2070–2079
54. Li R, Liu Q, Zhang R, Li Y, Ma Y, Huo H, Gao Y, Zuo P, Wang J, Yin G (2022) Achieving high-energy-density magnesium/sulfur battery via a passivation-free Mg–Li alloy anode. *Energy Storage Materials* 50:380–386
55. Wang P, Buchmeiser MR (2019) Rechargeable magnesium–sulfur battery technology: State of the art and key challenges. *Adv Func Mater* 29(49):1905248
56. Bieker G, Küpers V, Kolek M, Winter M (2021) Intrinsic differences and realistic perspectives of lithium–sulfur and magnesium–sulfur batteries. *Commun Mater* 2(1):37
57. Yao YY, Zhan Y, Sun XY, Li Z, Xu H, Laine RM, Zou JX (2023) Advances in cathodes for high-performance magnesium–sulfur batteries: A critical review. *Batteries* 9(4):203
58. Helen PA, Selvin PC, Sakthivel P (2024) Quasi-solid-state plasticized chitosan biopolymer electrolyte with enhanced Mg²⁺ ion mobility for next-generation Mg ion battery. *J Solid State Electrochem*. <https://doi.org/10.1007/s10008-024-05867-w>
59. Zhang J, Zeng Y, Li Q, Tang Z, Sun D, Huang D, Zhao L, Tang Y, Wang H (2023) Polymer-in-salt electrolyte enables ultrahigh ionic conductivity for advanced solid-state lithium metal batteries. *Energy Storage Mater* 54:440–449
60. Gao H, Grundish NS, Zhao Y, Zhou A, Goodenough JB (2021) Formation of stable interphase of polymer-in-salt electrolyte in all-solid-state lithium batteries. *Energy Mater Adv*. <https://doi.org/10.34133/2021/1932952>
61. Szczęśna-Chrzan A, Marczewski M, Syzdek J, Kochanec MK, Smoliński M, Marcinek M (2023) Lithium polymer electrolytes for novel batteries application: The review perspective. *Appl Phys A* 129(1):37
62. Yi C, Liu W, Li L, Dong H, Liu J (2019) Polymer-in-salt solid electrolytes for lithium-ion batteries. *Funct Mater Lett* 12(06):1930006
63. Tiruye GA, Munoz-Torrero D, Palma J, Anderson M, Marcilla R (2015) All-solid state supercapacitors operating at 3.5 V by using ionic liquid based polymer electrolytes. *J Power Sources* 279:472–480
64. Tiruye GA, Muñoz-Torrero D, Palma J, Anderson M, Marcilla R (2016) Performance of solid state supercapacitors based on polymer electrolytes containing different ionic liquids. *J Power Sources* 326:560–568
65. Pandey GP, Hashmi SA (2013) Solid-state supercapacitors with ionic liquid based gel polymer electrolyte: Effect of lithium salt addition. *J Power Sources* 243:211–218
66. Zheng S, Ma J, Wu ZS, Zhou F, He YB, Kang F, Cheng HM, Bao X (2018) All-solid-state flexible planar lithium ion microcapacitors. *Energy Environ Sci* 11(8):2001–2009
67. Khan Z, Ail U, Ajjan FN, Phopase J, Kim N, Kumar D, Khan ZU, Nilsson J, Inganäs O, Berggren M, Crispin X (2022) Towards printable water-in-polymer salt electrolytes for high power organic batteries. *J Power Sources* 524:231103
68. Khan Z, Ail U, Nadia Ajjan F, Phopase J, Ullah Khan Z, Kim N, Nilsson J, Inganäs O, Berggren M, Crispin X (2022) Water-in-polymer salt electrolyte for slow self-discharge in organic batteries. *Adv Energy Sustain Res* 3(1):2100165
69. Khan Z, Martinelli A, Franco LR, Kumar D, Idstrom A, Evenas L, Araujo CM, Crispin X (2023) Mass transport in “water-in-polymer salt” electrolytes. *Chem Mater* 35(16):6382–6395
70. Kumar D, Ail U, Wu Z, Björk EM, Berggren M, Gueskine V, Crispin X, Khan Z (2023) Zinc salt in “water-in-polymer salt electrolyte” for zinc–lignin batteries: electroactivity of the lignin cathode. *Adv Sustain Sys* 7(4):2200433
71. De Cachinho Cordeiro IM, Li A, Lin B, Ma DX, Xu L, Eh ALS, Wang W (2023) Solid polymer electrolytes for zinc-ion batteries. *Batteries* 9(7):343
72. Zhang J, Cui C, Wang PF, Li Q, Chen L, Han F, Jin T, Liu S, Choudhary H, Raghavan SR, Eidson N (2020) “Water-in-salt” polymer electrolyte for Li-ion batteries. *Energy Environ Sci* 13(9):2878–2887
73. Sundriyal S, Shrivastav V, Kaur A, Deep A, Dhakate SR (2021) Surface and diffusion charge contribution study of neem leaves derived porous carbon electrode for supercapacitor applications using acidic, basic, and neutral electrolytes. *J Energy Storage* 41:103000
74. Bouchemal N, Belhachemi M, Merzougui Z, Addoun F (2009) The effect of temperature and impregnation ratio on the active carbon porosity. *Desalin Water Treat* 10(1–3):115–120
75. Xie Y, Du H (2015) Electrochemical capacitance of a carbon quantum dots–polypyrrole/titania nanotube hybrid. *RSC Adv* 5(109):89689–89697
76. Zhang X, Peng C, Wang RT, Lang JW (2015) High-performance supercapacitors based on novel carbons derived from *Sterculia lychnophora*. *RSC Adv* 5(41):32159–32167
77. Xu W, Wang LM, Angell CA (2003) “PolyMOB”–lithium salt complexes: From salt-in-polymer to polymer-in-salt electrolytes. *Electrochim Acta* 48(14–16):2037–2045
78. Bae J, Li Y, Zhang J, Zhou X, Zhao F, Shi Y, Goodenough JB, Yu G (2018) A 3D nanostructured hydrogel-framework-derived high-performance composite polymer lithium-ion electrolyte. *Angew Chem Int Ed* 57(8):2096–2100
79. Zhu P, Yan C, Dirican M, Zhu J, Zang J, Selvan RK, Chung CC, Jia H, Li Y, Kiyak Y, Wu N (2018) Li_{0.33}La_{0.557}TiO₃ ceramic nanofiber-enhanced polyethylene oxide-based composite polymer electrolytes for all-solid-state lithium batteries. *J Mater Chem A* 6(10):4279–4285
80. Liu S, Liu W, Ba D, Zhao Y, Ye Y, Li Y, Liu J (2023) Filler-integrated composite polymer electrolyte for solid-state lithium batteries. *Adv Mater* 35(2):2110423
81. Ma Q, Liu D, Wang B, Liu W, Xiong G, Liu J (2023) Cellulose acetate-promoted polymer-in-salt electrolytes for solid-state

- lithium batteries. *J Solid State Electrochem* 27(6):1411–1421. <https://doi.org/10.1007/s10008-023-05414-z>
82. Tu H, Li L, Hu Y, Zhang Y, Wang Y, Huang W, Ren Z, Lin H, Liu M (2022) Non-flammable liquid polymer-in-salt electrolyte enabling secure and dendrite-free lithium metal battery. *Chem Eng J* 434:134647
 83. Jaumaux P, Yang X, Zhang B, Safaei J, Tang X, Zhou D, Wang C, Wang G (2021) Localized water-in-salt electrolyte for aqueous lithium-ion batteries. *Angew Chem Int Ed* 60(36):19965–19973
 84. Takada K, Yamada Y, Yamada A (2019) Optimized nonflammable concentrated electrolytes by introducing a low-dielectric diluent. *ACS Appl Mater Interfaces* 11(39):35770–35776
 85. Tiwari T, Pandey K, Srivastava N, Srivastava PC (2011) Effect of glutaraldehyde on electrical properties of arrowroot starch+NaI electrolyte system. *J Appl Polym Sci* 121(1):1–7
 86. Sing KS (1985) Reporting physisorption data for gas/solid systems with special reference to the determination of surface area and porosity (Recommendations 1984). *Pure Appl Chem* 57(4):603–619
 87. Zhang L, Lu S, Xiao D, Gu M (2017) Characterization of full pore size distribution and its significance to macroscopic physical parameters in tight glutenites. *J Nat Gas Sci Eng* 38:434–449
 88. Liu W, Yan X, Chen J, Feng Y, Xue Q (2013) Novel and high-performance asymmetric micro-supercapacitors based on graphene quantum dots and polyaniline nanofibers. *Nanoscale* 5(13):6053–6062
 89. Yadav M, Kumar M, Tiwari T, Srivastava N (2017) Wheat starch+ NaI: A high conducting environment friendly electrolyte system for energy devices. *Ionics* 23:2871–2880
 90. Conway BE, Conway BE (1999) Electrochemical behavior at porous electrodes; applications to capacitors. *Electrochemical Supercapacitors: Scientific Fundamentals and Technological Applications* 377–416. https://doi.org/10.1007/978-1-4757-3058-6_14
 91. Xu K, Ding SP, Jow TR (1999) Toward reliable values of electrochemical stability limits for electrolytes. *J Electrochem Soc* 146(11):4172
 92. Tien CP, Liang WJ, Kuo PL, Teng HS (2008) Electric double layer capacitors with gelled polymer electrolytes based on poly (ethylene oxide) cured with poly (propylene oxide) diamines. *Electrochim Acta* 53(13):4505–4511
 93. Liew CW, Ramesh S, Arof AK (2014) Good prospect of ionic liquid based-poly (vinyl alcohol) polymer electrolytes for supercapacitors with excellent electrical, electrochemical and thermal properties. *Int J Hydrogen Energy* 39(6):2953–2963
 94. Shilina Y, Levi MD, Dargel V, Aurbach D, Zavorine S, Nucciarone D, Humeniuk M, Halalay IC (2013) Ion size to pore width ratio as a factor that determines the electrochemical stability window of activated carbon electrodes. *J Electrochem Soc* 160(4):A629
 95. Alfaraño Serena R et al (2021) Stripping away ion hydration shells in electrical double-layer formation: Water networks matter. *Proc Natl Acad Sci* 118(47):e2108568118
 96. Ghosh S, Santhosh R, Jeniffer S, Raghavan V, Jacob G, Nanaji K, Kollu P, Jeong SK, Grace AN (2019) Natural biomass derived hard carbon and activated carbons as electrochemical supercapacitor electrodes. *Sci Rep* 9(1):16315
 97. Subramanian V, Luo C, Stephan AM, Nahm KS, Thomas S, Wei B (2007) Supercapacitors from activated carbon derived from banana fibers. *J Phys Chem C* 111(20):7527–7531
 98. Peng L, Peng X, Liu B, Wu C, Xie Y, Yu G (2013) Ultrathin two-dimensional MnO₂/graphene hybrid nanostructures for high-performance, flexible planar supercapacitors. *Nano Lett* 13(5):2151–2157
 99. Shao H, Wu YC, Lin Z, Taberna PL, Simon P (2020) Nanoporous carbon for electrochemical capacitive energy storage. *Chem Soc Rev* 49(10):3005–3039
 100. Simon P, Gogotsi Y (2010) Charge storage mechanism in nanoporous carbons and its consequence for electrical double layer capacitors. *Philosophical Transactions of the Royal Society A: Mathematical, Physical and Engineering Sciences* 368(1923):3457–3467
 101. Largeot C, Portet C, Chmiola J, Taberna PL, Gogotsi Y, Simon P (2008) Relation between the ion size and pore size for an electric double-layer capacitor. *J Am Chem Soc* 130(9):2730–2731
 102. Merlet C, Rotenberg B, Madden PA, Taberna PL, Simon P, Gogotsi Y, Salanne M (2012) On the molecular origin of supercapacitance in nanoporous carbon electrodes. *Nat Mater* 11(4):306–310
 103. Kötz R, Carlen MJE (2000) Principles and applications of electrochemical capacitors. *Electrochim Acta* 45(15–16):2483–2498
 104. Hsieh CT, Teng H (2002) Influence of oxygen treatment on electric double-layer capacitance of activated carbon fabrics. *Carbon* 40(5):667–674
 105. Ganesh B, Kalpana D, Renganathan NG (2008) Acrylamide based proton conducting polymer gel electrolyte for electric double layer capacitors. *Ionics* 14:339–343
 106. Singh MK, Suleman M, Kumar Y, Hashmi SA (2014) A novel configuration of electrical double layer capacitor with plastic crystal based gel polymer electrolyte and graphene nano-platelets as electrodes: A high rate performance. *Energy* 30:1–9
 107. Sun K, Feng E, Peng H, Ma G, Wu Y, Wang H, Lei Z (2015) A simple and high-performance supercapacitor based on nitrogen-doped porous carbon in redox-mediated sodium molybdate electrolyte. *Electrochim Acta* 158:361–367
 108. Mathis TS, Kurra N, Wang X, Pinto D, Simon P, Gogotsi Y (2019) Energy storage data reporting in perspective—guidelines for interpreting the performance of electrochemical energy storage systems. *Adv Energy Mater* 9(39):1902007
 109. Durukan MB, Keskin D, Tufan Y, Dincer O, Cicek MO, Yildiz B, Çınar Aygün S, Ercan B, Unalan HE (2023) An edible super [1]capacitor based on zwitterionic soy sauce-based gel electrolyte. *Adv Funct Mater* 34(6):2307051. <https://doi.org/10.1002/adfm.202307051>
 110. Zhao Z, Huang Y, Zheng H, Zhao L, Liu J, Zou C, Dong Z, Li X, Wang M, Lin Y (2023) Cotton fiber/PVA-based neutral hydrogel with Al³⁺ as an electrolyte additive for high-performance supercapacitors. *ACS Appl Energy Mater* 6(2):644–656
 111. Senokos E, Reguero V, Cabana L, Palma J, Marcilla R, Vilatela JJ (2017) Large-area, all-solid, and flexible electric double layer capacitors based on CNT fiber electrodes and polymer electrolytes. *Adv Mater Technol* 2(7):1600290
 112. Tooming T, Thomberg T, Kurig H, Jänes A, Lust E (2015) High power density supercapacitors based on the carbon dioxide activated d-glucose derived carbon electrodes and 1-ethyl-3-methylimidazolium tetrafluoroborate ionic liquid. *J Power Sources* 280:667–677
 113. Bhat MY, Hashmi SA (2019) Solid-state pseudocapacitors based on MnO₂ 2-nanorod-electrodes and plastic crystal incorporated gel polymer electrolyte: Synergistic effect of Li-salt addition in electrolyte and morphology of electrodes. *J Solid State Electrochem* 23:591–606

Publisher's Note Springer Nature remains neutral with regard to jurisdictional claims in published maps and institutional affiliations.

Springer Nature or its licensor (e.g. a society or other partner) holds exclusive rights to this article under a publishing agreement with the author(s) or other rightsholder(s); author self-archiving of the accepted manuscript version of this article is solely governed by the terms of such publishing agreement and applicable law.